Efficacy of diffeomorphic surface matching and 3D geometric morphometrics for taxonomic discrimination of Early Pleistocene hominin mandibular molars

José Braga [a, b, *], Veronika Zimmer [c, d], Jean Dumoncel [a], Chafik Samir [e], Frikkie de Beer [f], Clément Zanolli [a], Deborah Pinto [a], F. James Rohlf [g], Frederick E. Grine [g, h]

aComputer-assisted Palaeoanthropology Team, UMR 5288 CNRS-Université de Toulouse (Paul Sabatier), 37 Allées Jules Guesde, 31000 Toulouse, France
bEvolutionary Studies Institute, University of the Witwatersrand, Johannesburg 2050, South Africa
cDepartment of Anatomy, Faculty of Health Sciences, University of Pretoria, Pretoria 0001, South Africa
dDepartment of Biomedical Engineering, King's College London, London, UK
eLIMOS, UMR 6158 CNRS-Université Clermont Auvergne, 63173 Aubière, France
fSouth African Nuclear Energy Corporation (NECSA), Pelindaba, North West Province, South Africa
gDepartment of Anthropology, Stony Brook University, Stony Brook, NY 11794, USA
hDepartment of Anatomical Sciences, Stony Brook University, Stony Brook, NY 11794, USA

Abstract

Morphometric assessments of the dentition have played significant roles in hypotheses relating to taxonomic diversity among extinct hominins. In this regard, emphasis has been placed on the statistical appraisal of intraspecific variation to identify morphological criteria that convey maximum discriminatory power. Three-dimensional geometric morphometric (3D GM) approaches that utilize landmarks and semi-landmarks to quantify shape variation have enjoyed increasingly popular use over the past twenty-five years in assessments of the outer enamel surface (OES) and enamel–dentine junction (EDJ) of fossil molars. Recently developed diffeomorphic surface matching (DSM) methods that model the deformation between shapes have drastically reduced if not altogether eliminated potential methodological inconsistencies associated with the a priori identification of landmarks and delineation of semi-landmarks. As such, DSM has the potential to better capture the geometric details that describe tooth shape by accounting for both homologous and non-homologous (i.e., discrete) features, and permitting the statistical determination of geometric correspondence. We compare the discriminatory power of 3D GM and DSM in the evaluation of the OES and EDJ of mandibular permanent molars attributed to Australopithecus africanus, Paranthropus robustus and early Homo sp. from the sites of Sterkfontein and Swartkrans. For all three molars, classification and clustering scores demonstrate that DSM performs better at separating the A. africanus and P. robustus samples than does 3D GM. The EDJ provided the best results. P. robustus evinces greater morphological variability than A. africanus. The DSM assessment of the early Homo molar from Swartkrans reveals its distinctiveness from either australopith sample, and the "unknown" specimen from Sterkfontein (Stw 151) is notably more similar to Homo than to A. africanus.

Keywords

Sterkfontein, Swartkrans, *Australopithecus africanus, Paranthropus robustus*, Homo

1. Introduction

The sizes and shapes of teeth have been widely used to generate hypotheses relating to early hominin taxonomy and phylogeny. Traditionally, these studies have relied on linear morphometric variables, such as the mesiodistal and buccolingual diameters of tooth crowns, the planimetric areas occupied by molar cusps, and the subjective assessment of morphological features that manifest at the outer enamel surface (OES) of a tooth (e.g., Robinson, 1956; Coppens, 1980; Wood and Abbott, 1983; Grine, 1984, 1985, 1988, 1993; Wood and Uytterschaut, 1987; Wood and Engleman, 1988; Suwa, 1988, 1996; Suwa et al., 1996; Irish and Guatelli-Steinberg, 2003; Prat et al., 2005; Moggi-Cecchi et al., 2006, 2010; Moggi-Cecchi and Boccone, 2007; Martinón-Torres et al., 2008, 2012;

* Corresponding author.
E-mail addresses: jose.braga@univ-tlse3.fr (J. Braga), veronika.zimmer@upf.edu (V. Zimmer), jean.dumoncel@univ-tlse3.fr (J. Dumoncel), chafik.samir@udamail.fr (C. Samir), frikkie.debeer@necsa.co.za (F. de Beer), clement.zanolli@gmail.com (C. Zanolli), debora.impinto@gmail.com (D. Pinto), f.james.rohlf@stonybrook.edu (F.J. Rohlf), frederick.grine@stonybrook.edu (F.E. Grine).

Grine et al., 2009, 2013; Irish et al., 2013; Kaifu et al., 2015; Villmoare et al., 2015).

Over the past twenty-five years, such classic methods have been extended and supplemented by three-dimensional geometric morphometric (3D GM) approaches that utilize landmark and semi-landmark as well as landmark-free data to quantify shape variation (e.g., Bookstein, 1991; Rohlf and Marcus, 1993; O'Higgins, 2000; Adams et al., 2004, 2013; Slice, 2005, 2007; Mitteroecker and Gunz, 2009; Gunz and Mitteroecker, 2013). Landmark-based approaches entail the statistical analysis of shape variation and its covariation with other variables through the "Procrustes paradigm" where landmarks are superimposed to a common coordinate system. This approach has been widely applied in studies of the OES and enamel–dentine junction (EDJ) topographies of extant and fossil hominid dental samples (e.g., Martinón-Torres et al., 2006; Gómez-Robles et al., 2007, 2008, 2015; Skinner et al., 2008a, 2009a,b; Braga et al., 2010; Zanolli et al., 2012; Pan et al., 2016) and, owing to its relative success, has come to represent the current mainstream 3D approach to dental paleoanthropology.

Although 3D GM represents a powerful tool by which to assess morphological variation, assessments are based on correspondences between geometric features (anatomical landmarks) that have been specified a priori on the basis of observer expertise. As discussed below (see Methods), the main limitations of GM pertain to (i) the representation of shape by sets of homologous points, (ii) the use of a linear transformation for the matching procedure, and (iii) the definition and statistical analysis of shape differences that are based on the relative positions of individual landmark (and semi-landmark) points. A direct consequence is that 3D GM does not permit comparisons of differences that are related to local, non-homologous morphological features (e.g., presence versus absence of discrete trait such as a protostylid). Because non-homologous dental traits cannot be accounted for by 3D GM, they are commonly assessed separately using scoring systems such as the ASU dental reference plaques of Turner et al. (1991) (e.g., Skinner et al., 2008b, 2009c). The separate treatment of homologous and non-homologous features greatly hinders evaluation of their respective contributions to taxonomic discrimination within a single statistical framework. Indeed, it is not always obvious whether such categorical or quantitative data necessarily represent the best means by which to identify all relevant morphological information that can be extracted from either the OES or the EDJ of a tooth. Differing reliance on these data feeds the active debate over early hominin taxonomic diversity (e.g., Haile-Selassie et al., 2004, 2010; Clarke, 2013; Grine et al., 2013; Fornai et al., 2015).

As observed by MacLeod et al. (2010), the need to more fully automate morphological studies to determine geometric correspondence between shapes is a critical step that will enhance taxonomic studies. In their words, this might serve to "transform alpha taxonomy from a cottage industry dependent on the expertise of a few individuals to a testable and verifiable science accessible to anyone needing to recognize objects" (MacLeod et al., 2010: 154). Recent progress in 3D mathematical modeling and the development of surface matching methods (Boyer et al., 2011; Durrleman et al., 2012; Koehl and Hass, 2015) have permitted "the documentation of anatomical variation and quantitative traits with previously unmatched comprehensiveness and objectivity" (Boyer et al., 2011: 18226). In large measure, this has been through the elimination of inconsistencies in the prior choices of categorical features and landmarks. Diffeomorphisms is one of the surface matching methods that can capture 3D geometric details related to the cusps, basins, grooves, accessory cusps and ridges that define the shapes of teeth.

Surface matching using diffeomorphisms was first applied in evolutionary anthropology by Durrleman et al. (2012), who provided detail descriptions of the most important differences between diffeomorphic surface matching (DSM) and landmark-based 3D GM approaches. In comparison to 3D GM, diffeomorphic surface matching (DSM) models deformations between shapes that are represented as continuous surfaces rather than the positions of a relatively confined number of homologous points, and the matching process is based on anatomically "plausible" (i.e., smooth without tearing or folding), non-linear deformations (diffeomorphisms). While both 3D GM and DSM entail geometric approaches to morphometry, DSM utilizes geodesic distances, where the length of the geodesic provides a metric that measures the amount of diffeomorphic deformation. With DSM, shape differences are both defined by and statistically analyzed as deformations rather than by point positions, and this approach has been employed in several anthropological investigations (e.g., Koehl and Hass, 2015; Braga et al., 2016; Beaudet et al., 2016a, 2016b). In the present study, we utilize the DSM method of Durrleman et al. (2012, 2014) to investigate mandibular molar shape differences among South African Early Pleistocene hominins.

In order to assess the potential for DSM to recover novel data from early hominin teeth, we compare the results of analyses of dental shape obtained using both 3D GM and DSM methods. We also employ DSM to integrate homologous and non-homologous features in a single statistical framework so as to evaluate their respective contributions to intraspecific variation and taxonomic discrimination. Towards this end, we examine samples of lower permanent molars of *Australopithecus africanus* and *Paranthropus robustus* at both the OES and the EDJ. We further utilize these two methods to investigate the phenetic relationships of one specimen each from the sites of Swartkrans (SKX 257/258) and Sterkfontein (Stw 151) that have either been attributed or likened to early *Homo* sp. (Grine, 1989; Moggi-Cecchi et al., 1998).

2. Materials

The present study is based on micro-focal X-ray computed-tomography (micro-CT) data obtained for the three permanent lower molars (M_1, M_2 and M_3) of specimens attributed to *P. robustus* from the site of Swartkrans and to *A. africanus* from the site of Sterkfontein (Table 1). Unworn molars or those that exhibit minimal occlusal wear were chosen for study to maximize the number for which both the OES and EDJ could be modeled.

The *P. robustus* sample consists of 21 specimens, the majority of which derive from the Member 1 "Hanging Remnant" deposit. While most are represented at only a single tooth position, seven are represented by more than one molar. The attribution of the specimens to *P. robustus* by Robinson (1956), Grine (1988, 1989) and Grine and Daegling (1993) has enjoyed nearly universal acceptance by subsequent workers (e.g., Skinner et al., 2008a,b; Pan et al., 2016) with the sole exception of Schwartz and Tattersall (2003), who assigned SK 843 and SKX 4446 to *Homo* ("Morph 1"). However, Grine (2005) has demonstrated that the dimensions and shape of the mandibular corpus and the sizes of the P_4 and M_1 of SKX 4446 and the M_1 of SK 843 are consistent with their attribution to *Paranthropus* and unlike homologues of early *Homo*.

The Swartkrans sample also includes a single specimen from Member 2 (the SKX 257/258 M_1 antimeres) that has been attributed to *Homo* sp. by Grine (1989: 447) based on their relative BL narrowness, the presence of a moderate postmetaconulid (i.e., incipient tuberculum intermedium) and the absence of a tuberculum sextum. Grine's (1989) identification of SKX 257/258 has been accepted by all subsequent workers except Schwartz and Tattersall (2003), who misidentified the molars as deciduous rather than permanent (see Grine, 2005).

Table 1
Mandibular permanent molars from Sterkfontein and Swartkrans included in this study.

Site	Specimen	Provenience	Taxonomy	M_1		M_2		M_3	
				EDJ	OES	EDJ	OES	EDJ	OES
Swartkrans	SK 1	Mb. 1 HR	*P. robustus*			L	L		
	SK 6	Mb. 1 HR	*P. robustus*	L		L	L	L[b]	L[b]
	SK 23	Mb. 1 HR	*P. robustus*			L		L	
	SK 25	Mb. 1 HR	*P. robustus*	L	L	L	L		
	SK 61	Mb. 1 HR	*P. robustus*	R	R				
	SK 63	Mb. 1 HR	*P. robustus*	R	R	R[b]			
	SK 64	Mb. 1 HR	*P. robustus*	L[b]					
	SK 75	Mb. 1 HR	*P. robustus*					L	L
	SK 104	Mb. 1 HR	*P. robustus*	L	L				
	SK 828	Mb. 1 HR	*P. robustus*	R					
	SK 840	Mb. 1 HR	*P. robustus*					R	
	SK 843	Mb. 1 HR	*P. robustus*[a]	R		R		R	R
	SK 880	Mb. 1 HR	*P. robustus*					R	
	SK 1587	Mb. 1 HR	*P. robustus*			R			
	SK 3974	Mb. 1 HR	*P. robustus*	R	R				
	SKW 5	Mb. 1 HR	*P. robustus*	R		R	R	R	R
	SKX 257/258	Mb. 2	*Homo* sp.	R					
	SKX 4446	Mb. 2	*P. robustus*[a]	L		L	L		
Swartkrans	SKX 5002	Mb. 1 LB	*P. robustus*					R	
	SKX 5014	Mb. 1 LB	*P. robustus*					L	
	SKX 10642	Mb. 1 HR	*P. robustus*					R	R
	SKX 10643	Mb. 1 HR	*P. robustus*					R	R
Sterkfontein	Sts 24	Mb. 4	*A. africanus*	L	L				
	Sts 52	Mb. 4	*A. africanus*			R		R	R
	Stw 151	Mb. 5 ?	cf. *Homo*	R					
	Stw 309	Mb. 4	*A. africanus*	R					
	Stw 364	Mb. 4	*A. africanus*	R					
	Stw 404	Mb. 4	*A. africanus*			R		R	
	Stw 412	Mb. 4	*A. africanus*			R	R		
	Stw 421	Mb. 4	*A. africanus*	R	R				
	Stw 491	Mb. 4	*A. africanus*					L	
	Stw 529	Mb. 4	*A. africanus*			R			
	Stw 537	Mb. 4	*A. africanus*			L	L	L	L
	Stw 560	Mb. 4	*A. africanus*			R	R	L	L

Abbreviations: *P.* = *Paranthropus*; *A.* = *Australopithecus*; Mb = member; EDJ = enamel dentin junction; OES = outer enamel surface; R = right; L = left.
[a] Specimens erroneously attributed to *Homo* ("Morph 1") by Schwartz and Tattersall (2003); see Grine (2005).
[b] Incompletely developed crown near the cervical margin.

The *A. africanus* sample comprises 11 specimens from the Sterkfontein Member 4 deposit, and four of these are represented at more than one molar position. The attribution of these fossils to *A. africanus* by Robinson (1956) and Moggi-Cecchi et al. (2006) has seemingly enjoyed universal acceptance by subsequent workers. While Clarke (1988, 1994, 2008) has attributed a number of dental specimens from Sterkfontein to a second australopith species, *Australopithecus prometheus*, none of the fossils included in the current study have been so designated by him. Rather, Clarke (1988, 1994) has specifically referred two of the fossils in the current sample (Sts 52 and Stw 404) to *A. africanus*.

The Sterkfontein sample also includes one specimen (Stw 151) that comprises the associated teeth and skull fragments of a juvenile individual that likely derives from the same Member 5A deposit that yielded the Stw 53 *Homo* cranium. The Stw 151 composite was described by Moggi-Cecchi et al. (1998) as being more derived towards the early *Homo* condition than the rest of the *A. africanus* sample. Although Quam et al. (2013) attributed the specimen to *A. africanus* without explanation, Dean and Liversidge (2015) and Dean (2016) have adduced evidence pertaining to dental development that is more consistent with its assignation to *Homo* than *Australopithecus*.

A total of 24 teeth in the current sample (7 M_1s, 8 M_2s and 9 M_3s) exhibit no or minimal wear and revealed sufficient contrast between dentine and enamel to be used for morphometric analyses at both the OES and EDJ. Another 24 M (10 M_1s, 7 M_2s and 7 M_3s) were restricted to analysis of the EDJ because occlusal wear has obscured the pristine OES morphology.

3. Methods

All micro-CT (μCT) scans were performed using either the X-Tek XT H225L system (Metris) at the South African Nuclear Energy Corporation, Pelindaba (NECSA, www.necsa.co.za), or the XTH 225/320 LC dual source system (Nikon) at the Palaeosciences Centre, University of the Witwatersrand, Johannesburg. Isometric voxel dimensions ranged from 7.2 to 41 μm.

The μCT data were first imported into Avizo v7.0 (www.vsg3d.com/avizo) for segmentation and the reconstruction of the surface models (via triangulated "meshes" simplified to 100,000 faces) of either the EDJ or the OES (Fig. 1). In those instances where antimeres were present, the better-preserved crown was employed. In most cases, molars from the right side were used; in those instances where only the left molar was available, it was mirrored for subsequent computations using either 3D GM or DSM.

3.1. The 3D GM (landmark-based) approach

As noted above, 3D GM encodes shapes as represented by discrete, relatively small numbers of homologous landmarks and semi-landmarks configured either as Procrustes residuals or a matrix of partial warp scores. Although GM methodology currently represents the main 3D approach to study of dental morphology, there are several limitations associated with it. These relate specifically to 1) its restricted representation of shape, 2) the ability of its model to capture large deformations when partial warp scores are used to project the landmark data into Kendall's tangent space,

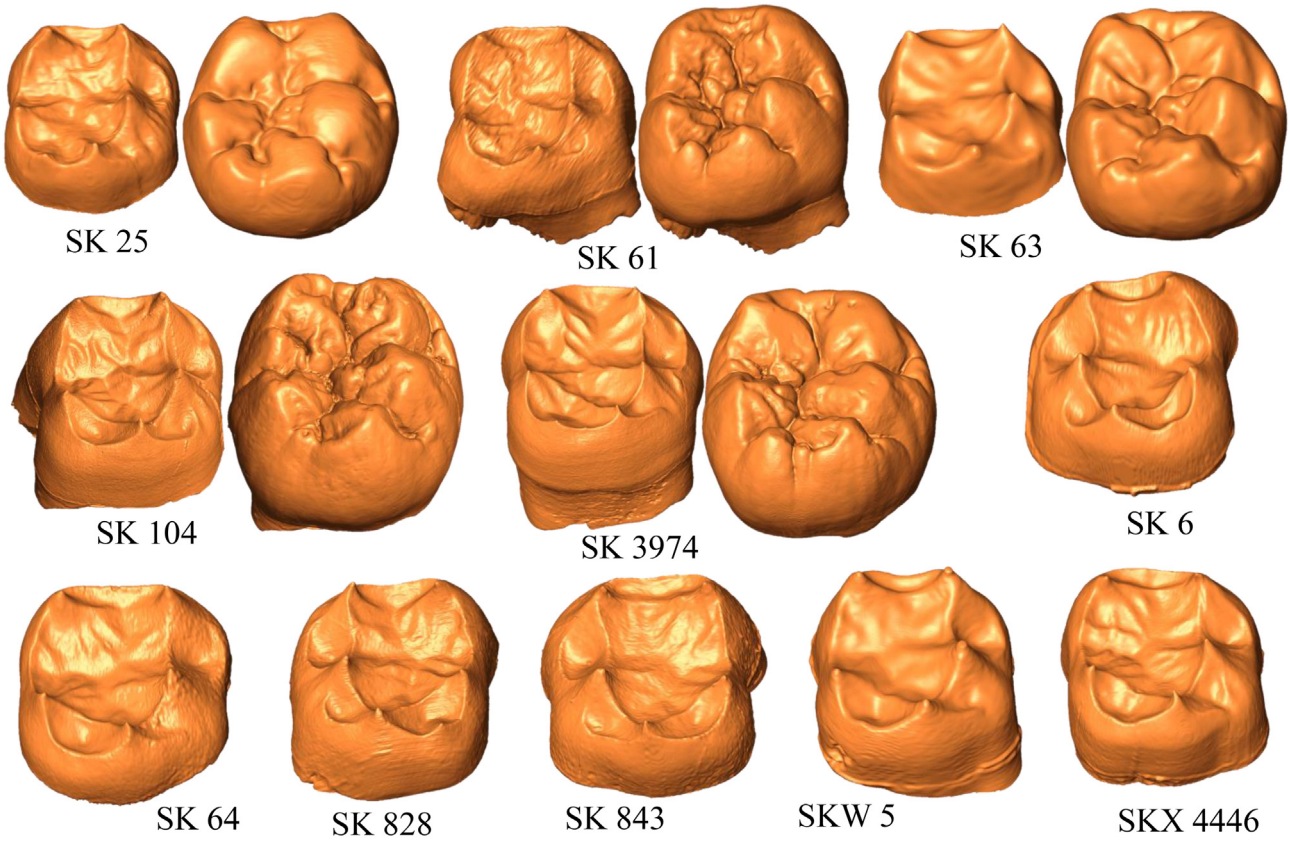
SK 25
SK 61
SK 63
SK 104
SK 3974
SK 6
SK 64
SK 828
SK 843
SKW 5
SKX 4446

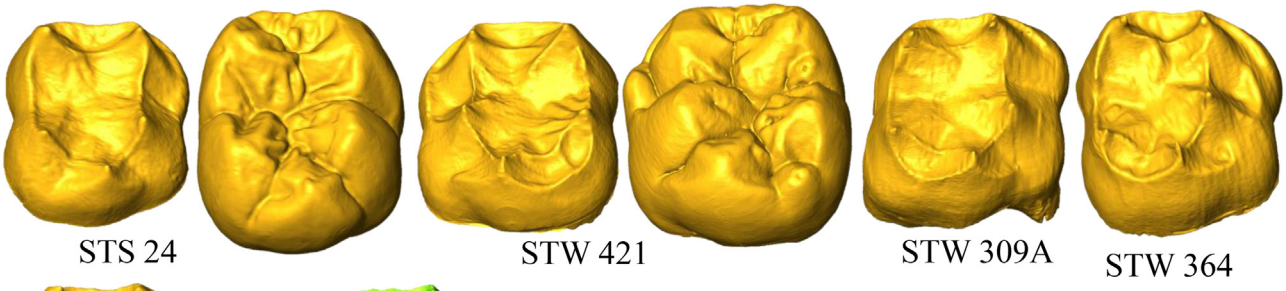
STS 24
STW 421
STW 309A
STW 364

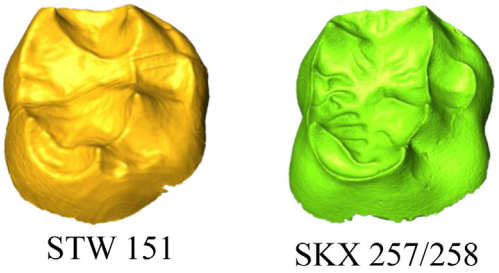
STW 151
SKX 257/258

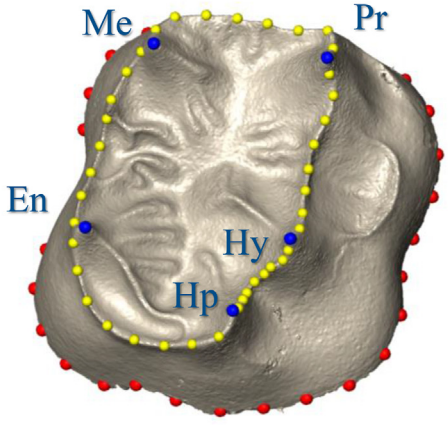
Me
Pr
En
Hy
Hp

and 3) its ability to define variability in shape when one or more surfaces comprise local non-homologous features. Each of these is briefly discussed below.

Shape representation GM represents shapes by means of a relatively limited set of homologous landmarks, and therefore it "cannot find changes within particular regions unless [there are] dense landmarks within them" (Zelditch et al., 2004: 28). In other words, because GM cannot capture morphology that is not encoded by the landmarks and semi-landmarks that have been selected in advance, its ability to analyze overall shape is limited.

Deformation model GM compares shapes by examining residuals after rigid matching (translation, rotation) and size scaling. These linear transformations, which are orthogonal transformations in a 3D Euclidean space, are global in nature. Therefore, even if GM is performed in a point-wise manner over entire surfaces that have been densely sampled (and no such study of this nature on teeth has been published to date), the performance of the rigid matching decreases in the face of non-homologous features. In other words, when shapes undergo large non-rigid deformations due to the occurrence of non-homologous features, rigid superimposition will necessarily lead to a poor fit and more often to a distortion of the surface. Furthermore, the measure of shape differences at any non-homologous region depends on the pattern of variation at its neighboring homologous areas. This limitation has been emphasized in a number of studies (e.g., Walker, 2000; Zelditch et al., 2004; von Cramon-Taubadel et al., 2007; Márquez et al., 2012) and is due to computing the residuals based on a quadratic measure of fit. Accordingly, differences that would lead to large residuals are reduced because a squared large residual will dominate the fitting process. In other words, least squares superimposition distributes local shape differences among 3D surfaces evenly across all landmarks. This is particularly evident when most of the shape differences occur at few landmark positions.

The point of note here is that GM requires homology in the sense that there must be correspondence between points that are considered to represent the same morphological manifestation.

Definition of shape variability The establishment of correspondences among definable homologous landmarks (as defined in Bookstein, 1991) is a prerequisite in GM. This means that any landmark that is identified on a particular form must be associated with its corresponding landmark on all the other geometric forms in the data set. Therefore, GM cannot properly compare two surfaces if one or both present local non-homologous (i.e., non-corresponding) features. This represents a potentially serious limitation in studies of the dentition, since any number of accessory grooves, pits, crests, crenulations and/or cusps that define surface shape may not necessarily be homologous between the surfaces being compared. Such variable features have been amply documented as being of taxonomic relevance among early hominin dentitions (e.g., Robinson, 1956; Coppens, 1980; Wood and Abbott, 1983; Grine, 1984, 1985, 1988, 1993; Wood and Uytterschaut, 1987; Wood and Engleman, 1988; Suwa, 1988, 1996; Suwa et al., 1996; Irish and Guatelli-Steinberg, 2003; Prat et al., 2005; Moggi-Cecchi et al., 2006, 2010; Moggi-Cecchi and Boccone, 2007; Martinón-Torres et al., 2008, 2012; Skinner et al., 2008b; Grine et al., 2009, 2013; Irish et al., 2013; Kaifu et al., 2015; Villmoare et al., 2015). Of course, information conveyed by some of these variable (non-homologous) structures may be of limited taxonomic and/or phylogenetic utility, but this same caveat applies equally to features defined by homologous sets of landmarks and/or semi-landmarks.

In the current study, we utilized 3D GM only in comparisons of the EDJ because it was not possible to reliably locate landmarks and semi-landmarks on the OES. With reference to the EDJ, two sets of landmarks and semi-landmarks were defined following the convention established by previous studies (e.g., Skinner et al., 2008a, 2009a; Braga et al., 2010). The first set included the dentine horn tips of the five principal cusps – protoconid, metaconid, entoconid, hypoconid and hypoconulid – as well as semi-landmarks located along the marginal ridges between these horn tips (Fig. 1). The second set comprised 30 semi-landmarks that delineated the cervical margin of the crown, beginning below the protoconid dentine horn (Fig. 1). In order to assess the influence of the template on the results, two separate GM analyses were conducted. In the first ("GM1"), only the first set of landmarks and semi-landmarks was employed. In the second ("GM2"), the two sets of landmarks and semi-landmarks were combined. Three incompletely developed molars (SK 64 M_1, SK 63 M_2, SK 6 M_3) were excluded from the GM2 analysis because the cervical margin had not yet been finalized at the time of death. The pattern of relationships in the landmark and semi-landmark configurations among the teeth were studied using principal component analysis (PCA).

3.2. The DSM (mesh-based) approach

The DSM approach establishes correspondences between surfaces by aligning them using local as well as global geometric features, and the difference between surfaces is interpreted as the amount of deformation needed to align them by using diffeomorphic shape matching (Durrleman et al., 2012). One of the main advantages of this method is its invariance to the extent to which non-homologous features are present in observed shapes. Furthermore, it is symmetric such that the deformation aligning shape A to shape B is the inverse of the deformation aligning shape B to shape A. This inverse relationship exists because the deformations are modeled as diffeomorphisms. As above, we present a discussion of the same three parameters as they relate to the application of DSM, namely 1) its representation of shape, 2) the ability of its model to capture deformations, and 3) its ability to define variability in shape when one or more surfaces comprise local non-homologous features.

Shape representation In DSM, shape is represented as a continuous surface. Each shape consists of an unordered set of points (vertices), edges (connections between two vertices) and faces (closed sets of edges) that jointly represent the surface in an explicit manner. Correspondences between surfaces are established through a kernel metric that considers all points on the surface without assuming any point-to-point correspondence (Durrleman, 2010). Importantly, this kernel metric represents the surface as vector fields and can be made insensitive to very small-scale surface variations that may occur due to segmentation errors or differing segmentation methods and that are not reproducible across individuals. Moreover, it does not depend on how the 3D meshes are sampled (numerically) and/or simplified by using different (larger or smaller) numbers of faces (Vaillant and Glaunès, 2005; Vaillant et al., 2007). This approach, which is widely applied in

Figure 1. EDJ and OES surface models of select M_1s from Swartkrans attributed to *P. robustus* (orange) or to early *Homo* (SKX 257/258) (green), and from Sterkfontein attributed to *A. africanus* or of debated affinity (Stw 151) (yellow). Stw 151 was treated as an unknown in the analyses. Note that the images are not to the same scale, but the relative sizes of EDJ to OES for any given tooth are to scale. The gray model at the bottom illustrates the placement of the landmarks at the tips of the dentine horns of the principal cusps (Me – metaconid, Pr – protoconid, En – entoconid, Hy – hypoconid, Hp – hypoconulid) (in blue), the semilandmarks on the ridges that course between them (in yellow) and along the cervix (in red). (For interpretation of the references to color in this figure legend, the reader is referred to the Web version of this article.)

the field of "computational anatomy" (Vaillant and Glaunès, 2005; Qiu et al., 2007; Vaillant et al., 2007; Durrleman et al., 2012), has the advantage of enabling direct computations of continuous and smooth deformations between two (or more) teeth that evince distinct morphologies even if the local features are not homologous.

Deformation model The deformations between two shapes are mathematically modeled as smooth and invertible functions referred to as diffeomorphisms. By using such functions, the topologies of the surfaces are preserved such that any deformation between them is anatomically "plausible" (i.e., smooth). The alignment of two surfaces using diffeomorphisms is obtained by optimizing an energy function. This procedure consists of maximizing the superimposition of the source surface onto the target surface as measured using the metric of currents, while constraining the deformation to be diffeomorphic. The consequence of the minimal energy principle and the topology-preserving constraint is that points belonging to the surface do not necessarily follow straight lines during deformation but may instead follow non-linear trajectories. The resulting diffeomorphisms rely on all data points represented on the continuous 3D surface without utilizing explicit point correspondences.

Definition of shape variability Analyses of the correspondence between two surfaces are based on the deformations (diffeomorphisms) between shapes rather than the correspondence between predetermined positions of points as it is the case with 3D GM. Vaillant et al. (2007) have demonstrated that DSM significantly improves matching in comparison to landmarks with regard to the measures of distances between surfaces in MRI scans. As such, DSM increases "the power of statistical testing of shape" (Vaillant et al., 2007: 17).

3.3. Statistical analyses

From the sample at each molar position (i.e., M_1, M_2 and M_3), a reference specimen was chosen at random, and all other specimens were rigidly aligned to its surface in position, rotation and scale. This was done by minimizing the root mean square distance between the points of each specimen to corresponding points on the reference surface using an iterative closest point algorithm. The Deformetrica software (www.deformetrica.org) (Durrleman et al., 2014) was then used to compute the diffeomorphisms separately for the EDJ and OES of the M_1, M_2 and M_3. The resulting diffeomorphisms were represented as vector fields describing the deformation at uniformly spaced control points. We then employed two distinct statistical approaches to analyzing the resultant differences among surfaces: 1) a pairwise approach combined with multidimensional scaling (MDS), and 2) a statistical atlas approach. Both of these are described below.

Pairwise approach In the pairwise approach, all the possible pairwise OES and EDJ diffeomorphisms were computed separately for the samples of the M_1, M_2 and M_3. Those diffeomorphisms are modeled as displacements of control-points to deform the underlying 3D space. A (symmetric) distance matrix was computed, where the pairwise deformation between any two specimens is computed from the average of the control-point displacements between them.

We employed a nonmetric, non-classical multidimensional scaling (MDS) (Cox and Cox, 2001), with a dimension of 3 and a stress normalized by the sum of the squares of the dissimilarities using Matlab in order to display the information contained in the pairwise distance matrices obtained for diffeomorphisms on the EDJ (Fig. 2; Supplementary Online Material (SOM) 1) and the OES (Fig. 3; SOM 2). Indeed, the goal of MDS is to reduce the dimensionality of a dataset (which consists of the relevant surfaces of all specimens) while preserving its intrinsic structure. New, low dimensional coordinates for each sample are based on a monotonic transformation of the pairwise distance matrix. In this regard, the aim of MDS is to optimize the location of each specimen in n-dimensional space where the dimensions (typically $n = 2$ or $n = 3$ for purposes of visualization) are specified a priori. The MDS then results in a new set of coordinates for each specimen. The proximity of specimens to one another in this low-dimensional space reflects how (dis)similar they are to one another in the original space of dense (high-dimensional) surfaces. In other words, the distances between pairs of specimens have the strongest possible relation to the dissimilarities among the pairs of 3D models that are compared using diffeomorphisms.

We present the PCA (for GM) and the MDS (for DSM) data using the first three dimensions (or modes) because this results in a better statistical fit than when two dimensions are employed. In order to evaluate and compare the GM and DSM approaches for morphological analysis of the EDJ, we analyze the low-dimensional spaces obtained by PCA and MDS (Fig. 2 and SOM 1). Ideally, such low-dimensional space should preserve distance structures between specimens. This means that similar shapes should map close together in the low-dimensional space and dissimilar shapes should map farther apart. All of the minimized stress values are below 15%, which indicates that the MDS data obtained using the first three dimensions conform well to the original distance matrices.

For a comparison of the discriminatory powers of DSM and GM, we performed clustering and classification experiments both in the high-dimensional shape spaces and in the low-dimensional embeddings. In the case of GM, the shape space consists of the landmark residuals after Procrustes alignment. Using the pairwise DSM approach, an explicit representation in shape space is not available and the symmetric distance matrix obtained by the mean deformation was used instead. We performed a hierarchical clustering and evaluated the homogeneity and completeness of the clusters with respect to taxonomic attributions using the V-measure (Rosenberg and Hirschberg, 2007). The V-measure registers values between 0 (poor clustering) and 1 (good quality clustering). In addition, we performed a k-nearest neighbor classification in the low-dimensional spaces to evaluate how well the class membership (i.e., the output in k-NN classification) distinguished the specimens according to their a priori taxonomic affiliation (i.e., either *A. africanus* or *P. robustus*). This was done using a leave-one-out cross-validation with $k = 3$, and evaluated with the balanced accuracy to account for class imbalance.

The MDS (for DSM) data of the OES for the three molars types of *P. robustus* and *A. africanus* are displayed graphically in Figure 3.

Statistical atlas approach The concept of a statistical atlas was introduced in medical imaging as a means by which to provide information on normative (multidimensional) morphological geometry and its variation in the description of shape (e.g., Chen, 1999; Chen et al., 1999; Däuber et al., 2002; Wu et al., 2009; Davatzikos and Verma, 2010; Fonseca et al., 2011). The statistical atlas represents a smooth probability map of the morphology of a given anatomical structure in a population, where that structure is modeled statistically using the sample of 3D meshes that represent it. The atlas enables the images from different individuals to be integrated in the same coordinate frame in a way that permits the norm and its variation to be visualized (Davatzikos and Verma, 2010). As such, it provides unique insight into the location(s) of the deviations from the morphological average.

A statistical atlas is constructed by aligning the 3D meshes into a reference, common coordinate system by iteratively applying

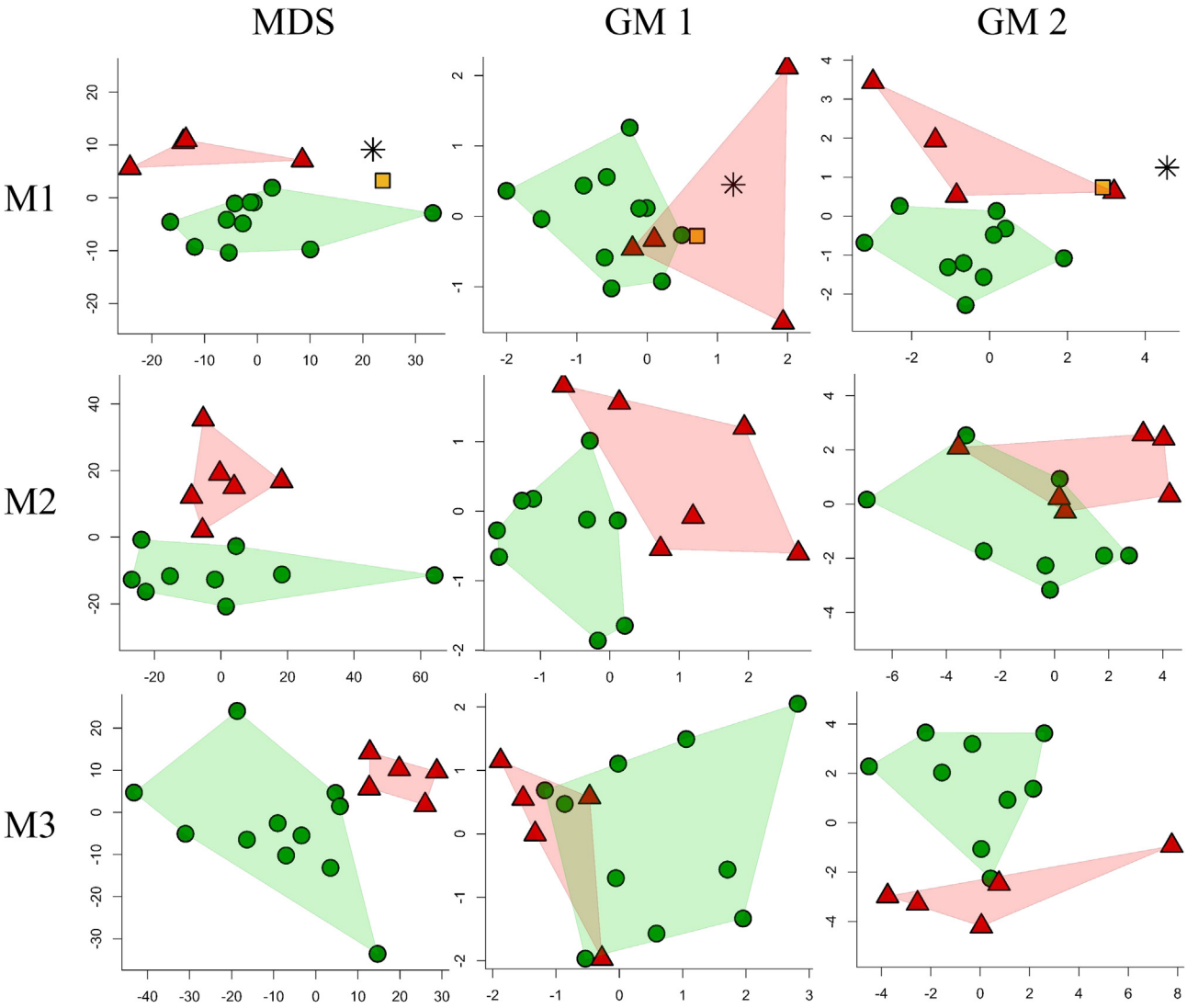

Figure 2. Results of multidimensional scaling (MDS) of DSM data (left column), principal components analysis (PCA) for GM1 data (middle column), and PCA for GM2 data (right column) obtained for the EDJ of M_1s (top row), M_2s (middle row) and M_3s (bottom row). Horizontal axis = mode 1; vertical axis = mode 2. *P. robustus* (green circles), *A. africanus* (red triangles). For visualization purposes, the SKW 257/258 early *Homo* M_1 (yellow square) and STW 151 M_1 (black star) are here projected onto the shape space to identify their closest neighbors. The minimized stress values are: 13.7% (M1, MDS), 10.4% (M2, MDS) and 12.9% (M3, MDS). The percentages of variances for modes 1 and 2 respectively are: 25.1% and 17.7% (M_1, GM1), 31.4% and 13.5% (M_1, GM2), 30.2% and 21.6% (M_2, GM1), 41.5% and 15.4% (M_2, GM2), 22.8% and 19.9% (M_3, GM1), and 30.0% and 24.4% (M_3, GM2). (For interpretation of the references to color in this figure legend, the reader is referred to the Web version of this article.)

diffeomorphisms. This establishes a function that is equivalent to numerical homology (Jardine and Jardine, 1967; Gao et al., 2018), which is equivalent to and has the same logical limitations as elliptical Fourier analysis of outline shapes (Rohlf and Archie, 1984; Rohlf, 1992). The geometrical variability within the sample of 3D meshes is estimated by first computing a mean surface (the "template"). When this mean shape is deformed onto each surface, the point distribution of the locations of the mesh vertices can be analyzed statistically. A statistical atlas encodes the geometrical variation within a sample by computing a 3D mesh that represents the mean shape and its principal "modes" of variation using the equivalent of principal component analysis (PCA) (Vaillant and Glaunès, 2005). In other words, a statistical atlas maps geometrical data from several individuals into one anatomical reference (i.e., a mean shape) so that the statistics of normal variability and deviations from it (i.e., the modes of variation) can be computed.

The construction of statistical atlases for the *A. africanus* or *P. robustus* samples followed this approach. In the first instance, mean shapes were computed for the *A. africanus* and *P. robustus* samples at each of the three molar positions (Fig. 4).

The clustering and classification results of the GM1/2 and DSM analyses were subsequently employed to ascertain whether the samples that were used to compute the statistical atlases were appropriate.

The atlases were also used to measure and display the geometrical variability among the surfaces for the first two modes of variation (i.e., dimensions 1 and 2; Miller, 2004; Bossa et al., 2007). This was illustrated by variability maps that combined the EDJ mean shape and its two associated extreme shapes at -2σ and $+2\sigma$ for modes 1 and 2, and the OES mean shape and its two associated extreme shapes at -2σ and $+2\sigma$ for modes 1 and 2 (Fig. 5). For each of the 12 means (i.e., for each australopith species sample, 3 means correspond to the EDJs and 3 means correspond to the OESs of the M_1, M_2 and M_3), the 'shape index' (Koenderink and van Doorn, 1992) was mapped on a color scale (convex minima in white; convex maxima in orange-brown, as shown in Fig. 5). The

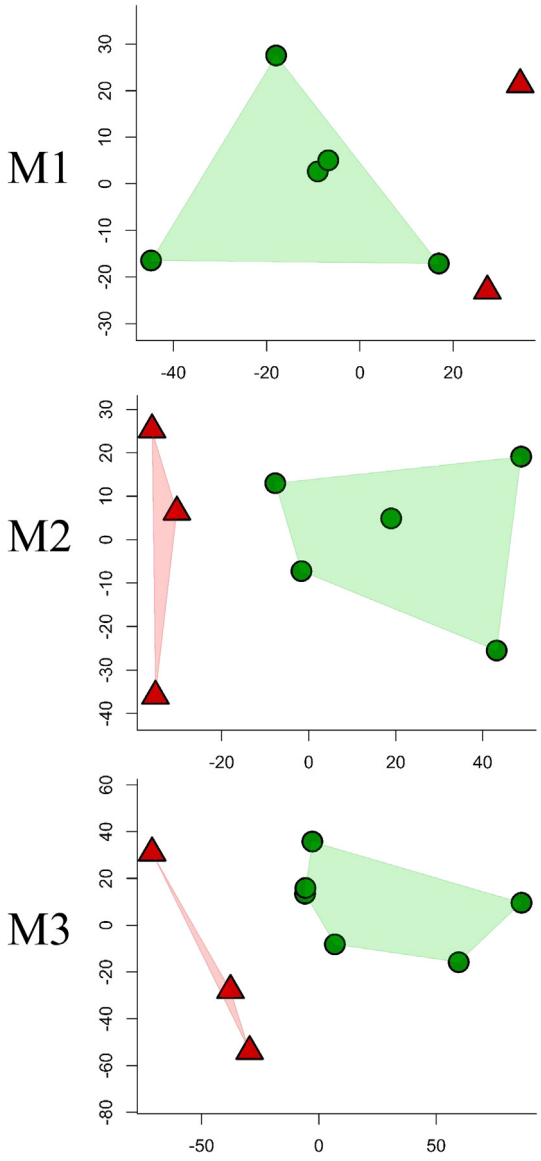

Figure 3. Results of multidimensional scaling (MDS) of DSM data for the OES of M_1s (top), M_2s (middle) and M_3s (bottom). Horizontal axis = mode 1; vertical axis = mode 2. *P. robustus* specimens (green circles) and *A. africanus* specimens (red triangles). The minimized stress values are: 7.7% (M1), 4.8% (M2) and 5.3% (M3). (For interpretation of the references to color in this figure legend, the reader is referred to the Web version of this article.)

shape index was calculated with Avizo ('GetCurvature' module) in order to measure locally the concave and convex minima and maxima. This measure is scale invariant and is represented by a number in the range [-1, +1] (a zero value indicates a saddle-like local structure (see Braga et al., 2010 for additional illustrations).

We compared the variability maps representing *A. africanus* or *P. robustus* samples to determine whether they showed the same patterns of variation. Shape differences between means and variation (Fig. 5) were illustrated with color maps (from dark blue to red illustrating the lowest and the highest differences, respectively). Statistical atlases were considered separately for the *A. africanus* and *P. robustus* samples for each molar position (M_1, M_2, M_3) and for each surface (EDJ or OES) in order to better visualize (i) the most distinctive morphological features between the two taxa (Fig. 4), and (ii) the most variable areas within each (Fig. 5).

4. Results

The degree to which the molars of *A. africanus* or *P. robustus* can be differentiated, and the degree to which the Swartkrans *Homo* (SKX 257/258) and Sterkfontein cf. *Homo* (Stw 151) specimens appear to differ from either are considered in relation to the performances of the 3D GM and DSM methods.

4.1. 3D GM (landmark-based) versus DSM (mesh-based) approaches

The representation of the diffeomorphism data with MDS with scatterplots of dimensions 1 and 2 reveals a clear separation between the *A. africanus* or *P. robustus* samples with regard to the EDJs of all three molars (Fig. 2). By comparison, the scores obtained from the GM1 and GM2 analyses along the first two PC axes do not discriminate the EDJs of these two samples as clearly (Fig. 2). According to the 3D GM analyses, the species samples are either in close proximity (M_1 with GM2, M_2 with GM1) to one another or they overlap somewhat (M_1 and M_3). With reference to the EDJs of the M_1 and M_2, the results obtained through the DSM and 3D GM approaches also differ when the data are represented in scatterplots of dimensions 2 and 3 (SOM 1 and 2). Here too, the MDS scatterplots discriminate *A. africanus* from *P. robustus* molars. The scores obtained along the PC2 and PC3 axes (SOM 1 and 2) do not discriminate with GM1, and while they perform better with GM2, the results are less clear than those obtained with DSM. The clustering and classification results obtained from the low-dimensional spaces for both approaches are provided in Table 2. The results from the low- and high-dimensional spaces are very similar for all methods, which indicates that PCA and MDS capture the most discriminatory information of shape spaces in only 3 dimensions. Below, we report the results obtained from the high-dimensional shape space, but similar conclusions are achieved with the low-dimensional space results.

It is also noteworthy that the V-measure, which corresponds to the strength of clustering, is higher for DSM than for either GM1 or GM2 for all three molars.

The results relating to the SKX 257/258 and Stw 151 first molars are noteworthy. In the first instance, the EDJ shape of SKX 257/258 is intermediate between *P. robustus* and *A. africanus* according to DSM, whereas both GM1 and GM2 data fail to discriminate it from the latter (Fig. 2). Secondly, the Stw 151 EDJ shape falls outside the envelope of *A. africanus* variation and is relatively close to SKX 257/258 according to the DSM analysis. On the other hand, the GM analyses find Stw 151 either situated comfortably within the *A. africanus* envelope (GM1), or beyond the *A. africanus* sample limits but with no particular affinity to SKX 257/258 (GM2) (Fig. 2). When compared to most australopith M_1 EDJs sampled in this study, both Stw 151 and SKX 257/258 exhibit a notable buccal expansion in the middle of the protoconid cingulum (Fig. 1).

Importantly, for both DSM and 3D GM, the best clustering results were obtained when the number of clusters was set to three. For all three molars, three clusters in the DSM shape space separated the Swartkrans sample into two groups (SOM 3). It is worth noting that Stw 151 and SKX 257/258 group together and are separated from the main *P. robustus* and *A. africanus* M_1 clusters (SOM 3). For all three molars, the clusters in the GM shape space were more heterogeneous (Table 2). The classification results also indicate a better separation between *A. africanus* and *P. robustus* when using DSM compared to either GM1 or GM2. In the GM2 analysis, the Stw 151 and SKX 257/258 M_1s group together but, in contrast to the DSM space, there is not a clear separation of the *A. africanus* and *P. robustus* samples. The low-dimensional DSM

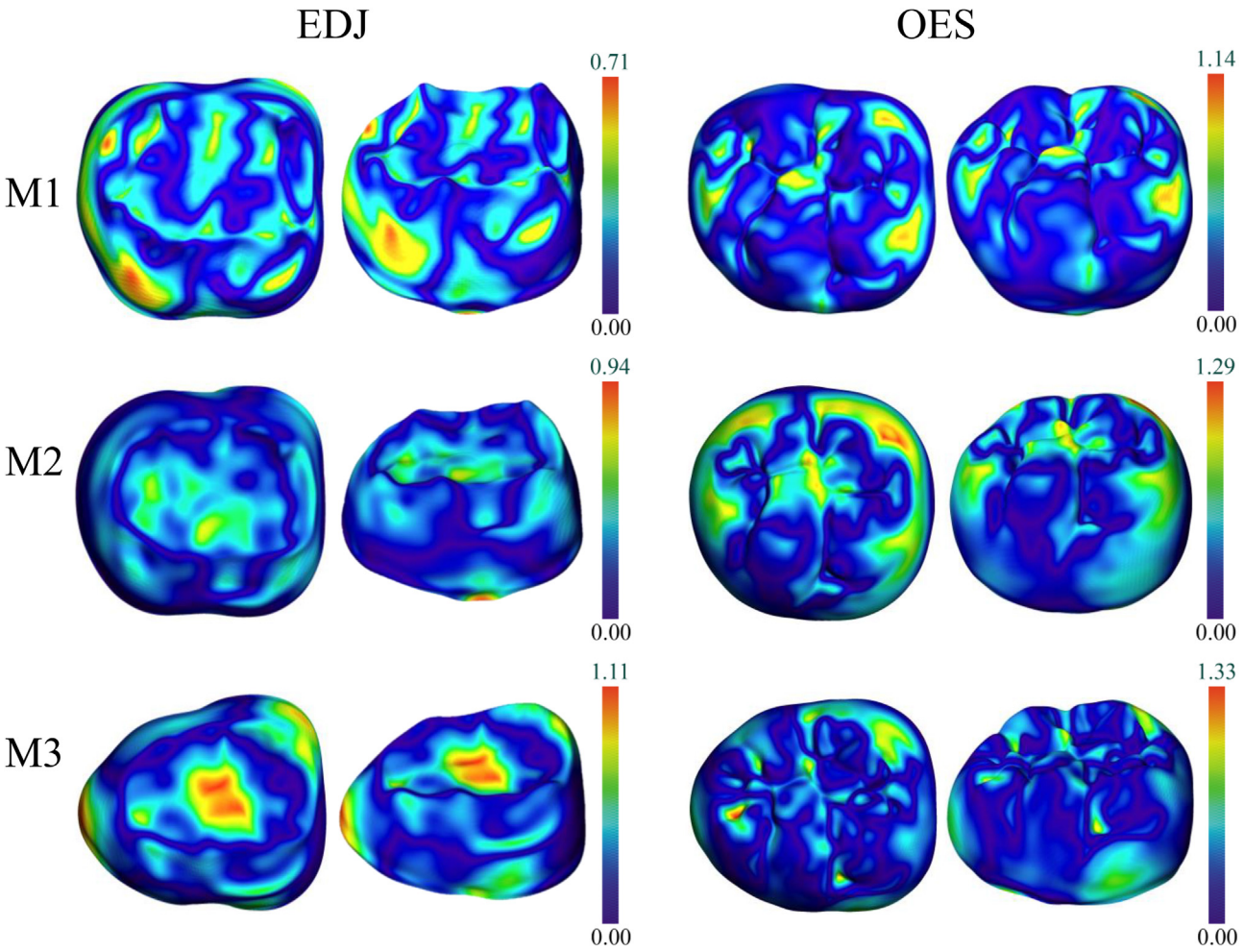

Figure 4. Color-coded differences between the *A. africanus* and *P. robustus* mean shapes of M_1, M_2 and M_3 EDJs and OESs computed with diffeomorphisms. The least and most distinct locations are indicated (in blue and red colors, respectively) on the *P. robustus* mean EDJ and OES shapes (left, occlusal view; right, oblique view). The scales are in mm. (For interpretation of the references to color in this figure legend, the reader is referred to the Web version of this article.)

space separated the specimens more accurately (Table 2). In this instance, a relatively low accuracy for M_1 EDJ classification was obtained using either GM (0.29 for GM1, 0.31 for GM2) or DSM (0.45) because Stw 151 and SKX 257/258 were considered to belong to neither *A. africanus* nor *P. robustus*. When Stw 151 and SKX 257/258 are excluded from comparison, accuracy increased for both methods (0.5 for GM1, 0.63 for GM2 and 0.88 for DSM (Table 2).

The mean GM2 configurations of the *A. africanus* and *P. robustus* M_1 EDJ semi-landmark Procrustes residuals attest to the higher dentine horns of the former (Fig. 6). Moreover, the entoconid and hypoconulid horns, the hypoconulid–hypoconid ridge, the mesiolingual and distobuccal angles of the cervix are more centrally placed, the mesial and distal marginal ridge is markedly lower (also on the M_2s), and the buccal extremity of the mesial marginal ridge is more squarely angled. With regard to the M_2 and M_3, the protoconid–hypoconid ridge projects more buccally, and the cervix is expanded between the mesial and distal roots in *A. africanus*. The mesial half of the metaconid–entoconid ridge projects more lingually on the *A. africanus* M_3, while on the M_3 of *P. robustus*, the distal marginal ridge and the distal moiety of the cervix are markedly expanded distally.

However, these differences between the *A. africanus* and *P. robustus* lower molar EDJs as computed with diffeomorphisms do not correspond to those illustrated by the landmark configurations (Fig. 4). For the M_1, the most important DSM differences are not located at the dentine horns or at the marginal ridges, but rather in three locations not sampled by landmarks and semi-landmarks in the GM approach (Fig. 4). These relate to i) a more bulging distobuccal slope of the hypoconid that is often associated with a marked distal protoconid ridge in *P. robustus* (the distobuccal corner of the *A. africanus* EDJ is more hollowed), (ii) a deeper mesiobuccal groove in *A. africanus*, and (iii) a more prominent distal marginal ridge that is commonly associated with one or two tuberculum sextum horns in *P. robustus*. However, these observations do not hold for the EDJ of the M_2 and M_3, where the most important differences between *A. africanus* and *P. robustus* are limited to the occlusal basins.

With reference to the OES of the molars, the scatterplots of dimensions 1 and 2 obtained from a MDS of DSM data show clear separation of *A. africanus* from *P. robustus* at all three molar positions (Fig. 3). When we compare the mean shapes of the *A. africanus* and *P. robustus* OES for all three molars, the most distinctive difference relates to the expanded mesiolingual slope of the metaconid in the former (Fig. 4). In addition, the M_1 of *A. africanus* is also rather distinct from that of *P. robustus* in the greater protrusion of the mesial slope of the protoconid (Fig. 4).

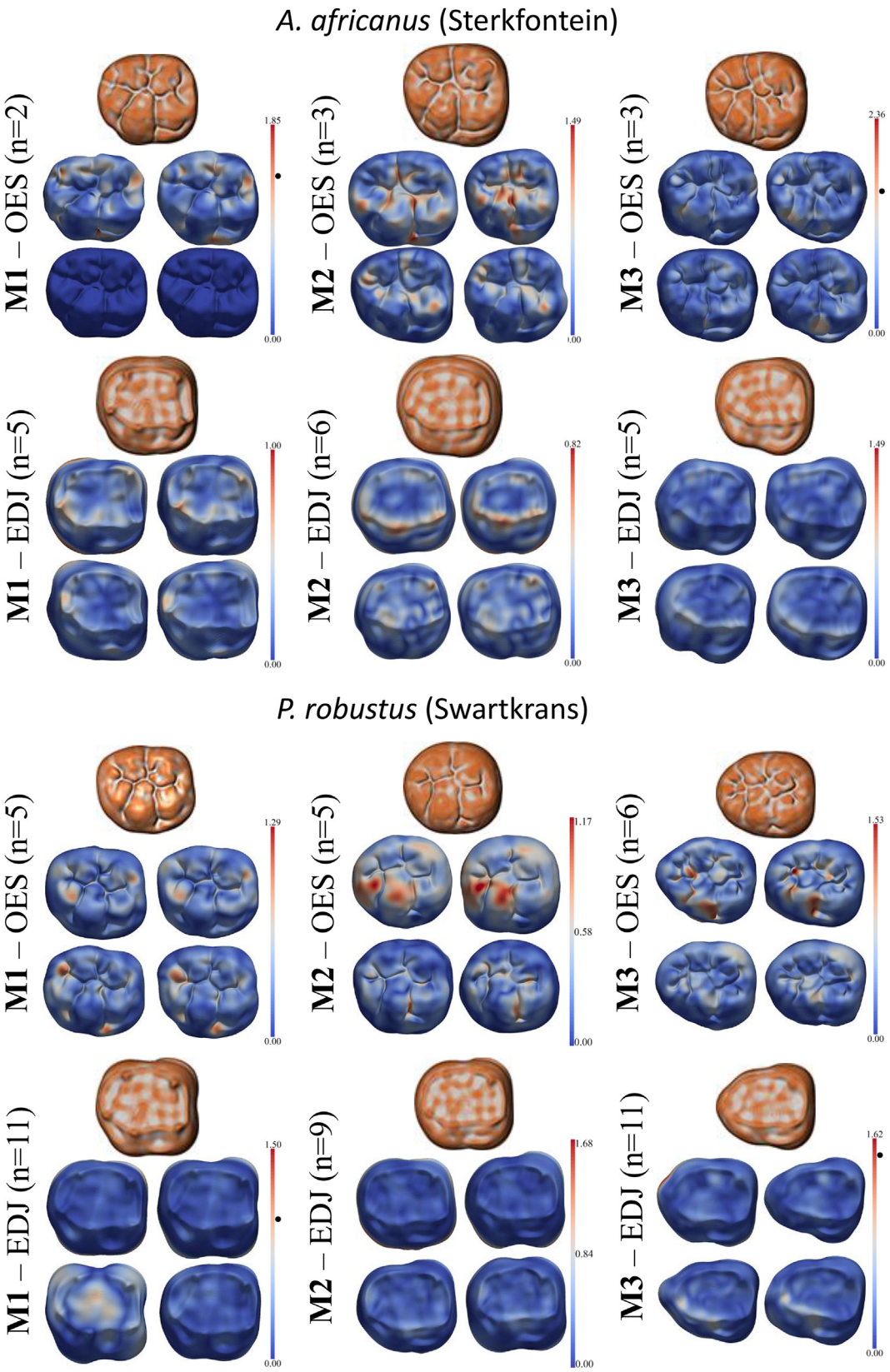

Figure 5. Statistical atlases with mean shapes (3D meshes illustrated in orange-brown) and associated extreme shapes (in the panels at the bottom of each mean shape) at -2σ (left) and $+2\sigma$ (right) obtained for the first (top row) and second (bottom row) modes of variation on the OES and EDJ of the M_1s, M_2s and M_3s of *A. africanus* and *P. robustus*. The variability (color-coded from blue to red) maps of both EDJ and OES illustrate the patterns of variations, i.e. the most (in red) and the least (in blue) variable areas for each surface. The scales are in mm. (For interpretation of the references to color in this figure legend, the reader is referred to the Web version of this article.)

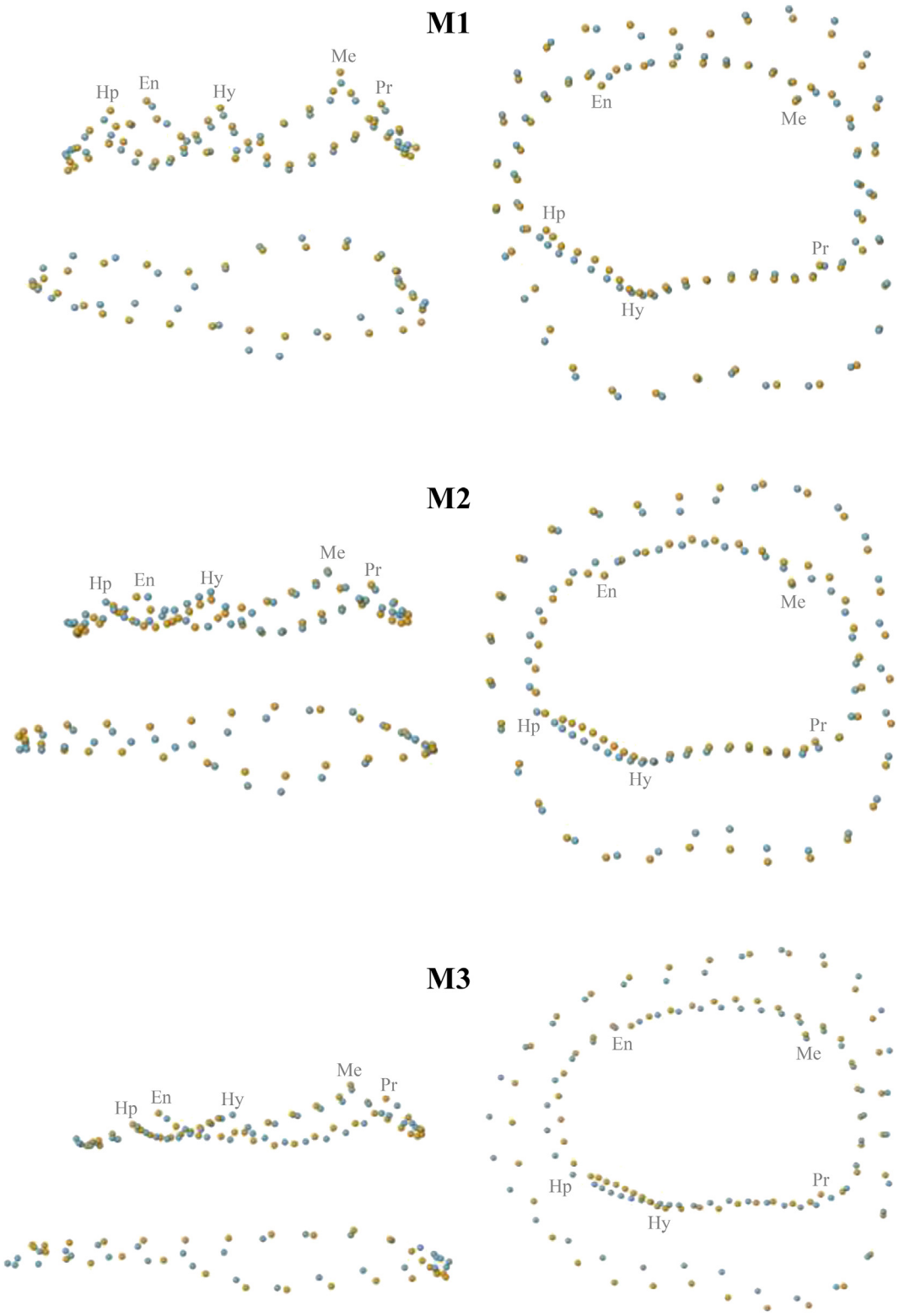

Figure 6. Mean configurations of *A. africanus* (orange) and *P. robustus* (blue) M_1s, M_2s and M_3s. Left = buccal view; Right = occlusal view. Mesial is to the right in all views. Pr, Protoconid; Hy, Hypoconid; Hp, Hypoconulid; En, Entoconid; Me, Metaconid. (For interpretation of the references to color in this figure legend, the reader is referred to the Web version of this article.)

4.2. Statistical atlases

Mean and extreme ($-/+2\sigma$) shapes Comparisons of the mean shapes among the different molar positions reveals greater metameric variation at the EDJ than the OES in both *A. africanus* and *P. robustus*. This is particularly evident in *P. robustus*, where the EDJ of the M_3 becomes nearly triangular. Indeed, comparison of the extremes of variation for each molar and for modes (or dimensions)

Table 2
Clustering and classification results obtained from the low-dimensional and high-dimensional spaces using either the geometric morphometric (GM) methods (GM1 with only landmarks and semi-landmarks at dentine horns and dentine crests; GM2 with additional semi-landmarks at cervix) or diffeomorphic surface matching (DSM) using diffeomorphisms and subsequent MDS analysis.

	Hierarchical clustering											
	Low-dimensional						High-dimensional					
	M_1		M_2		M_3		M_1		M_2		M_3	
	EDJ	OES	EDJ	OES	EDJ	OES	EDJ	OES	EDJ	OES	EDJ	OES
GM1	0.353		0.595		0.158		0.387		0.441		0.158	
GM2	0.417		0.271		0.489		0.448		0.271		0.489	
DSM	0.657	0.406	0.865	0.759	0.755	0.439	0.576	0.406	0.865	0.759	0.755	0.75
	Classification											
	Low-dimensional						High-dimensional					
	M_1		M_2		M_3		M_1		M_2		M_3	
	EDJ	OES	EDJ	OES	EDJ	OES	EDJ	OES	EDJ	OES	EDJ	OES
GM1	0.29 (0.5)		0.67		0.35		0.25 (0.5)		0.667		0.55	
GM2	0.313 (0.625)		0.56		0.74		0.25 (0.5)		0.771		0.744	
DSM	0.42 (0.88)	0.4	0.92	0.67	1	0.5	0.44 (0.88)	0.4	1	0.67	1	0.5

Clustering was evaluated using the V-measure, and classification was evaluated using balanced accuracy.
Abbreviations: EDJ = enamel dentin junction; OES = outer enamel surface.

1 and 2, reveals that *P. robustus* M_3s show the most extreme shape differences for mode 1 at both the EDJ and OES, becoming nearly triangular at -2σ for the OES and at $+2\sigma$ for the EDJ due to mesially expanded surfaces.

The variation between the two extremes is also noteworthy for *A. africanus* M_3s, but in this species, while the trigonid is buccolingually expanded at both the EDJ and the OES (for both modes 1 and 2), the talonid is less tapered than in *P. robustus*.

Patterns of variation The variability maps obtained for *A. africanus* and *P. robustus* (Fig. 5) can be examined separately for each molar to determine whether they reveal similar or dissimilar patterns at the EDJ and the OES. In order to illustrate the most and least variable areas for the two modes (or dimensions) obtained for each surface, we employ different color-coded scales to avoid the less variable areas (i.e., those with shorter scales) appearing completely uniform when compared to more variable surfaces (i.e., those with longer scales).

Overall, the extremes (at -2σ and $+2\sigma$) obtained for the first and second modes of variation reveal less variation at the EDJ than at the OES in both taxa (Fig. 5). In *P. robustus*, little variation is seen for the first mode computed for the EDJ at any of the three molar positions. This applies also to the second mode except that the surface computed for the M_1 at -2σ (higher variation mainly in the occlusal basin) and the M_3 at both -2σ and $+2\sigma$ (higher variation mainly on the hypoconid–hypoconulid ridge). When compared to *P. robustus*, the degree of EDJ variation observed for *A. africanus* is lower at all three molar positions (Fig. 5). Within *A. africanus*, the first mode of variation shows that the most variable areas are located at the metaconid and hypoconulid dentine horns on the M_1, and along the protoconid–hypoconid ridge on the M_2.

The variability maps obtained for the OES show very distinct patterns between *A. africanus* and *P. robustus* at each molar position. In the first mode of variation, *A. africanus* displays less variability than *P. robustus* in the M_3. The greatest variability in *P. robustus* is observed i) in the central part of the protoconid cingulum (for both the M_1 and the M_2), ii) in the main fissures of the occlusal basin of the M_2, and iii) in the mesial and distal foveae of the M_1. In *A. africanus*, for the second mode of variation, the M_2 OES appears most variable mainly at the protoconid and in the distal fovea. In *P. robustus*, for the first mode of variation, there is less OES variability relating to the fovea anterior and the hypoconulid of the M_1 and to the protostylid and the fissures of the occlusal basin of the M_2 whereas the hypoconid and hypoconulid of the M_2 are highly variable.

5. Discussion

5.1. Comparing 3D GM and DSM

Because landmarks and semi-landmarks cannot be reliably located on the OES, it was not possible to evaluate the ability of GM1 and GM2 approaches to distinguish between the *P. robustus* and *A. africanus* molar samples. Thus, comparisons of the efficacy of GM1/GM2 and DSM are restricted to the consideration of the EDJ. With reference to all three molar positions and both statistical approaches (i.e., the V-measure and the k-nearest neighbor classification), DSM resulted in clearer separation of the *A. africanus* and *P. robustus* samples when three groups were recognized (SOM 3).

Compared to the GM1/GM2 analyses, DSM applied to the EDJ of both the M_2 and M_3 did not mix *A. africanus* and *P. robustus* specimens into the same cluster, but instead clearly separated the two species. Here, all the *A. africanus* specimens were classified into a single cluster, while the *P. robustus* teeth were allocated to two other distinct clusters (SOM 3). The DSM allocation of the SK 63 M_2 to an "orphan" cluster (i.e., this tooth represents a cluster by itself) is very likely owing to its incomplete development at the cervical margin.

When applied to the EDJ of the M_1, DSM also separated most of the *A. africanus* and *P. robustus* specimens into two distinct clusters, but this analysis mixed SK 64, SK 6 and STS 24 into the same cluster with SKX 257/258 and Stw 151. While the DSM grouping of SKX 257/258 and Stw 151 with SK 64 may be due to the incompletely developed crown of the latter, the allocation of STS 24 and SK 6 to this cluster merits further attention. When applied to the M_1 EDJ, the GM1/GM2 approaches resulted in weaker classifications than DSM. Thus, GM1 separated SKX 257/258 and Stw 151 into two distinct clusters rather than one, and while GM2 grouped SKX 257/258 and Stw 151 with STS 24 (as did DSM), it failed to separate *A. africanus* and *P. robustus* into distinct clusters.

In contrast to the results of the GM1 and GM2 analyses, DSM (using both MDS and classifications) demonstrated unequivocally that the Stw 151 M_1 EDJ is significantly closer to the early *Homo*

condition as represented by SKX 257/258 than to the rest of the *A. africanus* sample from Sterkfontein Member 4 (Fig. 2 and SOM 3).

Koehl and Hass (2015) used three different anatomical datasets (including teeth) to compare clustering classifications using a DSM procedure and GM methods, and in all instances DSM was found to outperform GM. They ascribed this to "the difficulties in defining consistent landmarks on anatomical surfaces even for experienced morphometricians" (Koehl and Hass, 2015: 8). Even if one were to argue that EDJ presents easily identifiable landmarks (e.g., sharp dentine horns), it is noteworthy that the most distinctive differences between *A. africanus* and *P. robustus* EDJs that were defined by DSM (Fig. 4) could not be identified by GM methods. For example, the expansion of the distobuccal face of the hypoconid in *P. robustus* M_1s contributes significantly to the high statistical accuracy of their distinction from *A. africanus* homologues. Another important difference between GM and DSM lies in the latter's visualization of morphological variability within a sample, and the ability to compute statistical atlases using DSM. Importantly, the MDS and the classifications obtained in this study confirmed the a priori taxonomic attributions (Table 1).

5.2. Incorporating categorical features into 3D shape analyses

In addition to the degree to which the distobuccal surface of the hypoconid of the *P. robustus* M_1 EDJ is expanded, two other regions of this tooth are distinctive between *A. africanus* and *P. robustus*, and both correspond to what have been described as "discrete" features. The first relates to the greater prominence of the distal marginal ridge on the *P. robustus* M_1, which corresponds to the (variably-sized) tuberculum sextum that is manifest at the OES in much higher frequencies in this species than in *A. africanus* (Wood and Abbott, 1983; Irish and Guatelli-Steinberg, 2003; Grine et al., 2012; Irish et al., 2013). The second relates to the shallower mesiobuccal groove on the EDJ in *P. robustus*, and this corresponds to differences in the expression of the protostylid between it and *A. africanus* at both OES and EDJ (Robinson, 1956; Sperber, 1974; Hlusko, 2004; Skinner et al., 2008a).

Qualitative analyses of discrete dental features among early hominins have sometimes resulted in different interpretations owing to differing definitions and scoring methods, and to questions of homology. This study has demonstrated that DSM enables the 3D quantification of such discrete, possibly non-homologous entities that provide teeth with their individuality. As such, DSM may help to overcome the difficulties associated with the subjective scoring of discrete features.

5.3. Future perspectives

The differences between the *A. africanus* and the *P. robustus* samples described in this study, together with the clear and separate clustering of Stw 151 with the SK 257/258 early *Homo* M_1 represent encouraging developments for the employment of DSM in taxonomic and morphologic assessment. However, the samples that were employed here must be augmented with other specimens that have been attributed to these taxa to more fully assess the potential of DSM to address taxonomic issues. Thus, for example, the present study did not entail investigation of possible differences among Sterkfontein and Makapansgat specimens with reference to suggestions that they attest to the presence of more than one species of *Australopithecus* (cf.., Clarke, 1988, 1994, 2008; Moggi-Cecchi and Boccone, 2007; Fornai et al., 2015; Grine, 2013; Grine et al., 2013). Similarly, this study did not include the important fossils from the sites of Kromdraai, Drimolen and Gondolin that are attributed to *P. robustus*, but for which there have been suggestions of some morphological differences (e.g., Howell, 1978; Grine, 1985, 1988, 1993; Kaszycka, 2002; Braga et al., 2013, 2017).

The confirmation of the distinctiveness of Stw 151 from the *A. africanus* sample (Moggi-Cecchi et al., 1998) and its attribution to *Homo* through the application of DSM techniques has important implications for the analysis of other Early Pleistocene specimens that have been purported to be members of our genus. In particular, DSM could be applied fruitfully to questions relating to the attribution of fossils to *Homo habilis* and *H. rudolfensis* and to the taxonomic relationships of the South African *Homo* specimens (Grine et al., 2019).

Finally, a more comprehensive DSM examination of the South African australopith samples, together with the inclusion of additional fossils that have been attributed (or at least likened) to early *Homo* from these and Pleistocene sites in South Africa may help clarify questions that have been raised concerning the affinities of recently described forms such as *Australopithecus sediba* (e.g., Berger et al., 2010; Wood and Harrison, 2011; Been and Rak, 2014; Rak and Been, 2014; Ritzman et al., 2016; Kimbel and Rak, 2017) and *Homo naledi* (Berger et al., 2015, 2017; Hawks et al., 2017; Neves et al., 2017; Schroeder et al., 2017).

Acknowledgments

This work was supported by the Erasmus Mundus "AESOP plus" programme of the European Union, the French Ministry of Foreign Affairs, the French Embassy in South Africa through the Cultural and Cooperation Services, the Centre National de la Recherche Scientifique and the HPC resources of the CALMIP Supercomputing Centre. FEG and FJR were additionally supported by the College of Arts and Sciences, Stony Brook University. We thank Stephany Potze, Ditsong Museum, Pretoria, and Bernhard Zipfel and the Fossil Access Committee of the University of the Witwatersrand, Johannesburg, for access to specimens. We are also grateful to Jakobus Hoffman and Jakata Kudakwashe for their help with scanning at the South African Nuclear Energy Corporation, Pelindaba (NECSA) and the Palaeosciences Centre Microfocus X-ray Computed Tomography (CT) Facility at the University of the Witwatersrand. We thank Mike Plavcan, the associate editor and two anonymous reviewers for their helpful comments that improved the manuscript.

References

Adams, D.C., Rohlf, F.J., Slice, D.E., 2004. Geometric morphometrics: ten years of progress following the "revolution". Italian Journal of Zoology 71, 5–16. Adams,
D.C., Rohlf, F.J., Slice, D.E., 2013. A field comes of age: geometric morphometrics in the 21st Century. Hystrix 24, 7–14.
Beaudet, A., Dumoncel, J., Thackeray, J.F., Bruxelles, L., Duployer, B., Tenailleau, C., Bam, L., Hoffman, J., de Beer, F., Braga, J., 2016a. Upper third molar inner structural organization and semicircular canal morphology in Plio-Pleistocene South-African cercopithecoids. Journal of Human Evolution 95, 104–120.
Beaudet, A., Dumoncel, J., de Beer, F., Duployer, B., Durrleman, S., Gilissen, E., Hoffman, J., Tenailleau, C., Thackeray, J.F., Braga, J., 2016b. Morphoarchitectural variation in South African fossil cercopithecoid endocasts. Journal of Human Evolution 101, 65–78.
Been, E., Rak, Y., 2014. The lumbar spine of *Australopithecus sediba* indicates two hominid taxa. Paleoanthropology (abstract A12).
Bookstein, F.L., 1991. Morphometric Tools for Landmark Data: Geometry and Biology. Cambridge University Press, Cambridge.
Berger, L.R., de Ruiter, D.J., Churchill, S.E., Schmid, P., Carlson, K.J., Dirks, P.H.G.M., Kibii, J.M., 2010. *Australopithecus sediba*: a new *Homo*-like australopith from South Africa. Nature 328, 195–204.
Berger, L.R., Hawks, J., de Ruiter, D.J., Churchill, S.E., Schmid, P., Delezene, L.K., Kivell, T.L., Garvin, H.M., Williams, S.A., DeSilva, J.M., Skinner, M.M., Musiba, C.M., Cameron, N., Holliday, T.W., Harcourt-Smith, W., Ackermann, R.R.,

Bastir, M., Bogin, B., Bolter, D., Brophy, J., Cofran, Z.D., Congdon, K.A., Deane, A.S., Dembo, M., Drapeau, M., Elliott, M.C., Feuerriegel, E.M., Garcia-Martinez, D., Green, D.J., Gurtov, A., Irish, J.D., Kruger, A., Laird, M.F., Marchi, D., Meyer, M.R., Nalla, S., Negash, E.W., Orr, C.M., Radovcic, D., Schroeder, L., Scott, J.E., Throckmorton, Z., Tocheri, M.W., VanSickle, C., Walker, C.S., Wei1, P., Zipfel, B., 2015. *Homo naledi*, a new species of the genus *Homo* from the Dinaledi Chamber, South Africa. eLife 4, e09560.

Berger, L.R., Hawks, J., Dirks, P.H.G.M., Elliott, M., Roberts, E.M., 2017. *Homo naledi* and Pleistocene hominin evolution in subequatorial Africa. eLife 6, e24234. Bossa, M., Hernandez, M., Olmos, S., 2007. Contributions to 3D diffeomorphic atlas estimation: application to brain images. In: Medical Image Computing and Computer-Assisted Intervention. MICCAI. Series Lecture Notes in Computer Science, vol. 4791, pp. 667–674.

Boyer, D.M., Lipman, Y., St Clair, E., Puente, J., Patel, B.A., Funkhouser, T., Jernvall, J., Daubechies, I., 2011. Algorithms to automatically quantify the geometric simi-larity of anatomical surface. Proceedings of the National Academy of Sciences of the United States of America 108, 18221–18226.

Braga, J., Thackeray, J.F., Subsol, G., Kahn, J.-L., Maret, D., Treil, J., Beck, A., 2010. The enamel–dentine junction in the postcanine dentition of *Australopithecus africanus*: intra-individual metameric and antimeric variation. Journal of Anatomy 216, 62–79.

Braga, J., Thackeray, J.F., Dumoncel, J., Descouens, D., Bruxelles, L., Loubes, J.-M., Kahn, J.L., Stampanoni, M., Bam, L., Hoffman, J., de Beer, F., Spoor, F., 2013. A new partial temporal bone of a juvenile hominin from the site of Kromdraai B (South Africa). Journal of Human Evolution 65, 447–456.

Braga, J., Dumoncel, J., Duployer, B., Tenailleau, C., de Beer, F., Thackeray, J.F., 2016. The Kromdraai hominins revisited with an updated portrayal of differences between *Australopithecus africanus* and *Paranthropus robustus*. In: Braga, J., Thackeray, J.F. (Eds.), Kromdraai, a Birthplace of *Paranthropus* in the Cradle of Humankind. Sun Media Metro, Johannesburg, pp. 49–68.

Braga, J., Thackeray, J.F., Bruxelles, L., Dumoncel, J., Fourvel, J.-B., 2017. Stretching the time span of hominin evolution at Kromdraai (Gauteng, South Africa): recent discoveries. Comptes Rendus Palevol 16, 58–70.

Chen, M., 1999. 3-D Deformable registration using a statistical atlas with applications in medicine. PhD Dissertation. Carnegie Mellon University.

Chen, M., Kanade, T., Pomerleau, D., Schneider, J., 1999. 3-D deformable registration of medical images using a statistical atlas. In: Taylor, C., Colchester, A. (Eds.), Medical Image Computing and Computer-Assisted Intervention – MICCAI 1999. Springer, Berlin, pp. 621–630.

Clarke, R.J., 1988. A new *Australopithecus* cranium from Sterkfontein and its bearing on the ancestry of *Paranthropus*. In: Grine, F.E. (Ed.), Evolutionary History of the "Robust" Australopithecines. Aldine de Gruyter, New York, pp. 285–292.

Clarke, R.J., 1994. Advances in understanding the craniofacial anatomy of South African early hominids. In: Corruccini, R.S., Ciochon, R.L. (Eds.), Integrative Paths to the Past. Paleoanthropological Advances in Honor of F. Clark Howell. Prentice Hall, Englewood Cliffs, NJ, pp. 205–222.

Clarke, R.J., 2008. Latest information on Sterkfontein's *Australopithecus* skeleton and a new look at *Australopithecus*. South African Journal of Science 104, 443–449.

Clarke, R.J., 2013. *Australopithecus* from Sterkfontein caves, South Africa. In: Reed, K.E., Fleagle, J.G., Leakey, R.E. (Eds.), The Paleobiology of *Australopithecus*. Springer, New York, pp. 105–123.

Coppens, Y., 1980. The differences between *Australopithecus* and *Homo*: preliminary conclusions from the Omo Research Expedition's studies. In: K¨onigsson, L.K.(Ed.), Current Argument on Early Man. Pergamon, Oxford, pp. 207–225.

Cox, T.F., Cox, M.A.A., 2001. Multidimensional Scaling. Chapman and Hall/CRC Monographs on Statistics & Applied Probability, Boca Raton.

Dauber, S., Krempien, R., Kr¨atz, M., Welzel, T., Wo¨rn, H., 2002. Creating a statistical atlas of the cranium. Studies in Health Technology and Informatics 85, 116–120.

Davatzikos, C., Verma, R., 2010. Statistical Atlases. In: Bryan, N. (Ed.), Introduction to the Science of Medical Imaging. Cambridge University Press, Cambridge, pp. 240–249.

Dean, M.C., Liversidge, H.M., 2015. Age estimation in fossil hominins: comparing dental development in early *Homo* with modern humans. Annals of Human Biology 42, 415–429.

Dean, M.C., 2016. Measures of maturation in early fossil hominins: events at the first transition from australopiths to early *Homo*. Philosophical Transactions of the Royal Society B, Biolological Sciences 371, 20150234.

Durrleman, S., 2010. Statistical models of currents for measuring the variability of anatomical curves, surfaces and their evolution. Thesis. University of Nice – Sophia Antipolis.

Durrleman, S., Pennec, X., Trouv´e, A., Ayache, N., Braga, J., 2012. Comparison of the endocranial ontogenies between chimpanzees and bonobos via temporal regression and spatiotemporal registration. Journal of Human Evolution 62, 74–88.

Durrleman, S., Prastawa, M., Charon, N., Korenberg, J.R., Joshi, S., Gerig, G., Trouv´e, A., 2014. Morphometry of anatomical shape complexes with dense deformations and sparse parameters. NeuroImage 101, 35–49.

Fonseca, C.G., Backhaus, M., Bluemke, D.A., Britten, R.D., Chung, J.D., Cowan, B.R., Dinov, I.D., Finn, J.P., Hunter, P.J., Kadish, A.H., 2011. The Cardiac Atlas Project – an imaging database for computational modeling and statistical atlases of the heart. Bioinformatics 27, 2288–2295.

Fornai, C., Bookstein, F.L., Weber, G.W., 2015. Variability of *Australopithecus* second maxillary molars from Sterkfontein Member 4. Journal of Human Evolution 85, 181–192.

Gao, T.R., Yapuncich, G.S., Daubechies, I., Mukherjee, S., Boyer, D.M., 2018. Development and assessment of fully automated and globally transitive geometric morphometric methods, with application to a biological comparative dataset with high interspecific variation. Anatomical Record 301, 636–658.

G´omez-Robles, A., Martin´on-Torres, M., Bermúdez de Castro, J.M., Margvelashvili, A., Bastir, M., Arsuaga, J.L., P´erez-P´erez, A., Estebaranz, F., Martínez, L.M., 2007. A geometric morphometric analysis of hominin upper first molar shape. Journal of Human Evolution 53, 272–285.

G´omez-Robles, A., Martin´on-Torres, M., Bermúdez de Castro, J.M., Prado, S., Sarmiento, S., Arsuaga, J.L., 2008. Geometric morphometric analysis of the crown morphology of the lower first premolar of hominins, with special attention to Pleistocene *Homo*. Journal of Human Evolution 55, 627–638.

G´omez-Robles, A., Bermúdez de Castro, J.M., Martin´on-Torres, M., Prado-Sim´on, L., Arsuaga, J.L., 2015. A geometric morphometric analysis of hominin lower molars: evolutionary implications and overview of postcanine dental variation. Journal of Human Evolution 82, 34–50.

Grine, F.E., 1984. Comparison of the deciduous dentitions of Africa and Asian hominids. Courier Forschungsinstitut Senckenberg 69, 69–82.

Grine, F.E., 1985. Australopithecine evolution: the deciduous dental evidence. In: Delson, E. (Ed.), Ancestors: the Hard Evidence. Alan R. Liss, New York, pp. 153–167.

Grine, F.E., 1988. New craniodental fossils of *Paranthropus* from the Swartkrans formation and their significance in 'robust' australopithecine evolution. In: Grine, F.E. (Ed.), Evolutionary History of the 'Robust' Australopithecines. Aldine de Gruyter, New York, pp. 223–243.

Grine, F.E., 1989. New hominid fossils from the Swartkrans Formation (1979–1986 excavations): craniodental specimens. American Journal of Physical Anthropology 79, 409–449.

Grine, F.E., 1993. Description and preliminary analysis of new hominid craniodental fossils from the Swartkrans Formation. In: Brain, C.K. (Ed.), Swartkrans. A Cave's Chronicle of Early Man. Transvaal Museum, Pretoria, pp. 75–116.

Grine, F.E., 2005. Early *Homo* at Swartkrans, South Africa: a review of the evidence and an evaluation of recently proposed morphs. South African Journal of Sciences 101, 43–52.

Grine, F.E., 2013. The alpha taxonomy of *Australopithecus africanus*. In: Reed, K.E.,Fleagle, J.G., Leakey, R.E. (Eds.), The Paleobiology of *Australopithecus*. Springer, Dordrecht, pp. 73–104.

Grine, F.E., Daegling, D.J., 1993. New mandible of *Paranthropus robustus* from Member 1, Swartkrans Formation, South Africa. Journal of Human Evolution 24, 319–333.

Grine, F.E., Smith, H.F., Heesy, C.P., Smith, E.J., 2009. Phenetic affinities of Plio-Pleistocene *Homo* fossils from South Africa: molar cusp proportions. In: Grine, F.E., Fleagle, J.G., Leakey, R.E. (Eds.), The First Humans. Origin and Early Evolution of the Genus *Homo*. Springer, New York, pp. 49–62.

Grine, F.E., Jacobs, R.L., Reed, K.E., Plavcan, J.M., 2012. The enigmatic molar from Gondolin, South Africa: implications for *Paranthropus* paleobiology. Journal of Human Evolution 63, 597–609.

Grine, F.E., Delanty, M.M., Wood, B.A., 2013. Variation in mandibular postcanine dental morphology and hominin species representation in Member 4, Sterk-fontein, South Africa. In: Reed, K.E., Fleagle, J.G., Leakey, R.E. (Eds.), The Paleo-biology of Australopithecus. Springer, New York, pp. 125–146.

Grine, F.E., Leakey, M.G., Gathago, P.N., Brown, F.H., Mongle, C.S., Yang, D., Jungers, W.L., Leakey, L.N., 2019. Complete permanent mandibular dentition of early *Homo* from the upper Burgi Member of the Koobi Fora Formation, Ileret, Kenya. Journal of Human Evolution (in press).

Gunz, P., Mitteroecker, P., 2013. Semilandmarks: a method for quantifying curves and surfaces. Hystrix 24, 103–109.

Haile-Selassie, Y., Suwa, G., White, T.D., 2004. Late Miocene teeth from Middle Awash, Ethiopia, and early hominid dental evolution. Science 303, 1503–1505.

Haile-Selassie, Y., Saylor, B.Z., Deino, A., Alene, M., Latimer, B.M., 2010. New hominid fossils from Woranso-Mille (Central Afar, Ethiopia) and taxonomy of early *Australopithecus*. American Journal of Physical Anthropology 141, 406–417. Hawks, J., Elliott, M., Schmid, P., Churchill, S.E., de Ruiter, D.J., Roberts, E.M., Hilbert-Wolf, H., Garvin, H.M., Williams, S.A., Delezene, L.K., Feuerriegel, E.M., Randolph-Quinney, P., Kivell, T.L., Laird, M.F., Tawane, G., DeSilva, J.M., Bailey, S.E., Brophy, J.K., Meyer, M.R., Skinner, M.M., Tocheri, M.W., VanSickle, C., Walker, C.S., Campbell, T.L., Kuhn, B., Kruger, A., Tucker, S., Gurtov, A., Hlophe, N., Hunter, R., Morris, H., Peixotto, B., Ramalepa, M., van Rooyen, D., Tsikoane, M., Boshoff, P., Dirks, P.H.G.M., Berger, L.R., 2017. New fossil remains of *Homo naledi* from the Lesedi Chamber, South Africa. eLife 6, e24232.

Hlusko, L.J., 2004. Protostylid variation in *Australopithecus*. Journal of Human Evolution 46, 579–594.

Howell, F.C., 1978. Hominidae. In: Maglio, V.J., Cooke, H.B.S. (Eds.), Evolution of African Mammals. Harvard University Press, Cambridge, pp. 154–248.

Irish, J.D., Guatelli-Steinberg, D., 2003. Ancient teeth and modern human origins: an expanded comparison of African Plio-Pleistocene and recent world dental samples. Journal of Human Evolution 45, 113–144.

Irish, J.D., Guatelli-Steinberg, D., Legge, S.S., de Ruiter, D.J., Berger, L.R., 2013. Dental morphology and the phylogenetic "place" of *Australopithecus sediba*. Science 340, 1233062-1-4.

Jardine, N., Jardine, C.J., 1967. Numerical homology. Nature 216, 301–302.

Kaifu, Y., Kono, R.T., Sutikna, T., Saptomo, E.W., Jatmiko, D.A.R., 2015. Unique dental morphology of *Homo floresiensis* and its evolutionary implications. PLoS ONE 10(11) e0141614.

Kaszycka, K.A., 2002. Status of Kromdraai: cranial, mandibular and dental morphology, systematic relationships, and significance of the Kromdraai Hominids. In: Editions du Cahiers de Pal´eoanthropologie. CNRS, Paris. Kimbel, W.H., Rak, Y., 2017. *Australopithecus sediba* and the emergence of *Homo*: Questionable evidence from the cranium of the juvenile holotype MH 1. Journal of Human Evolution 107, 94–106.

Koehl, P., Hass, J., 2015. Landmark-free geometric methods in biological shape analysis. Journal of the Royal Society Interface 12, 20150795.

Koenderink, J.J., van Doorn, A.J., 1992. Surface perception in pictures. Perceptions and Psychophysics 52, 487–496.

MacLeod, N., Benfield, M., Culverhouse, P., 2010. Time to automate identification. Nature 467, 154–155.

Marquez, E.J., Cabeen, R., Woods, R.P., Houle, D., 2012. The measurement of local variation in shape. Evolutionary Biology 39, 419–439.

Martin´on-Torres, M., Bastir, M., Bermúdez de Castro, J.M., G´omez, A., Sarmiento, S., Muela, A., Arsuaga, J.L., 2006. Hominin lower second premolar morphology: evolutionary inferences through geometric morphometric analysis. Journal of Human Evolution 50, 523–533.

Martin´on-Torres, M., Bermúdez de Castro, J., G´omez-Robles, A., Margvelashvili, A., Prado, L., Lordkipanidze, D., Vekua, A., 2008. Dental remains from Dmanisi (Republic of Georgia): morphological analysis and comparative study. Journal of Human Evolution 55, 249–273.

Martin´on-Torres, M., de Castro, J.M.B., G´omez-Robles, A., Prado-Simon, L., Arsuaga, J.L., 2012. Morphological description and comparison of the dental remains from Atapuerca-Sima de los Huesos site (Spain). Journal of Human Evolution 62, 7–58.

Miller, M., 2004. Computational anatomy: shape, growth, and atrophy comparison via diffeomorphisms. NeuroImage 23, S19–S33.

Mitteroecker, P., Gunz, P., 2009. Advances in geometric morphometrics. Evolutionary Biology 36, 235–247.

Moggi-Cecchi, J., Boccone, S., 2007. Maxillary molars cusp morphology of South African australopithecines. In: Bailey, S.E., Hublin, J.J. (Eds.), Dental Perspectives on Human Evolution: State-of-the-Art Research in Dental Paleoanthropology. Springer, Dordrecht, pp. 53–64.

Moggi-Cecchi, J., Tobias, P.V., Beynon, A.D., 1998. The mixed dentition and associated skull fragments of a juvenile fossil hominid from Sterkfontein, South Africa. American Journal of Physical Anthropology 106, 425–465.

Moggi-Cecchi, J., Grine, F.E., Tobias, P.V., 2006. Early hominid dental remains from Members 4 and 5 of the Sterkfontein Formation (1966–1996 excavations): catalogue, individual associations, morphological descriptions and initial metrical analysis. Journal of Human Evolution 50, 239–328.

Moggi-Cecchi, J., Menter, C.G., Boccone, S., Keyser, A.W., 2010. Early hominin dental remains from the Plio-Pleistocene site of Drimolen, South Africa. Journal of Human Evolution 58, 374–405.

Neves, W.A., Bernardo, D.V., Pantaleoni, I., 2017. Morphological affinities of *Homo naledi* with other Plio-Pleistocene hominins: a phonetic approach. Anais da Academia Brasileira de Ci^encias 89(3 Suppl.), 2199–2207.

O'Higgins, P., 2000. The study of morphological variation in the hominid fossil record: biology, landmarks and geometry. Journal of Anatomy 197, 103–120.

Pan, L., Dumoncel, J., de Beer, F., Hoffman, J., Thackeray, J.F., Duployer, Tenailleau, C., Braga, J., 2016. Further morphological evidence on South African earliest *Homo* lower postcanine dentition: enamel thickness and enamel dentine junction. Journal of Human Evolution 96, 82–96.

Prat, S., Brugal, J.P., Tiercelin, J.J., Barrat, J.A., Bohn, M., Delagnes, A., Harmand, S., Kimeu, K., Kibunjia, M., Texier, P.J., Roche, H., 2005. First occurrence of early *Homo* in the Nachukui Formation (West Turkana, Kenya) at 2.3–2.4 Myr. Journal of Human Evolution 49, 230–240.

Qiu, A., Younes, L., Wang, L., Ratnanather, J.T., Gillepsie, S.K., Kaplan, G., Csernansky, J., Miller, M., 2007. Combining anatomical manifold information via diffeomorphic metric mappings for studying cortical thinning of the cingulate gyrus in schizophrenia. Neuroimage 37, 821–833.

Quam, R.M., de Ruiter, D.J., Masali, M., Arsuaga, J.-L., Martínez, I., Moggi-Cecchi, J., J., 2013. Early hominin auditory ossicles from South Africa. Proceedings of the National Academy of Sciences of the United States of America 110, 8847–8851.

Rak, Y., Been, E., 2014. Two hominid taxa and Malapa: the mandibular evidence. Paleoanthropology (abstract A20).

Ritzman, T.B., Terhune, C.E., Gunz, P., Robinson, C.A., 2016. Mandibular ramus shape of *Australopithecus sediba* suggests a single variable species. Journal of Human Evolution 100, 54–64.

Robinson, J.T., 1956. The Dentition of the Australopithecinae. Transvaal Museum Memoir 9. Transvaal Museum, Pretoria.

Rohlf, F.J., 1992. The analysis of shape variation using ordinations of fitted functions. In: Sorensen, J.T. (Ed.), Ordinations in the Study of Morphology, Evolution and Systematics of Insects: Applications and Quantitative Genetic Rationales. Elsevier, Amsterdam, pp. 95–122.

Rohlf, F.J., Archie, J.W., 1984. A comparison of Fourier methods for the description of wing shape in mosquitoes (Diptera: Culicidae). Systematic Zoology 33, 302–317.

Rohlf, F.J., Marcus, L.F., 1993. A revolution in morphometrics. Trends in Ecology and Evolution 8, 129–132.

Rosenberg, A., Hirschberg, J., 2007. V-measure: a conditional entropy-based external cluster evaluation measure. In: Proceedings of Joint Conference on Empirical Methods in Natural Language Processing and Computational Natural Language Learning, pp. 410–420.

Schroeder, L., Scott, J., Garvin, H., Laird, M.F., Dembo, M., Radov˘ci´c, D., Berger, L.R., de Ruiter, D.J., Ackermann, R.R., 2017. Skull diversity in the *Homo* lineage and the relative position of *Homo naledi*. Journal of Human Evolution 104, 124–135.

Schwartz, J.H., Tattersall, I., 2003. The human fossil record. In: Craniodental Morphology of Genus *Homo* (Africa and Asia), vol. 2. Wiley-Liss, NewYork, pp. 409–449.

Skinner, M.M., Gunz, P., Wood, B.A., Hublin, J.J., 2008a. Enamel–dentine junction (EDJ) morphology distinguishes the lower molars of *Australopithecus africanus* and *Paranthropus robustus*. Journal of Human Evolution 55, 979–988. Skinner, M.M., Wood, B., Boesch, C., Olejniczak, A.J., Rosas, A., Smith, T.M., Hublin, J.J., 2008b. Dental trait expression at the enamel–dentine junction of lower molars in extant and fossil hominoids. Journal of Human Evolution 54, 173–186.

Skinner, M.M., Gunz, P., Wood, B., Boesch, C., Hublin, J.J., 2009a. Discrimination of extant *Pan* species and subspecies using the enamel–dentine junction morphology of lower molars. American Journal of Physical Anthropology 140, 234–243.

Skinner, M.M., Gunz, P., Wood, B.A., Hublin, J.J., 2009b. How many landmarks? Assessing the classification accuracy of *Pan* lower molars using a geometric morphometric analysis of the occlusal basin as seen at the enamel–dentine junction. Frontiers of Oral Biology 13, 23–29.

Skinner, M.M., Wood, B.A., Hublin, J.J., 2009c. Protostylid expression at the enamel–dentine junction and enamel surface of mandibular molars of *Paranthropus robustus* and *Australopithecus africanus*. Journal of Human Evolution 56, 76–85.

Slice, D.E., 2005. Modern morphometrics. In: Slice, D.E. (Ed.), Modern Morphometrics in Physical Anthropology. Kluwer Press, New York, pp. 1–45.

Slice, D.E., 2007. Geometric morphometrics. Annual Review of Anthropology 36, 261–281.

Sperber, G.H., 1974. Morphology of the cheek teeth of Early South African hominids. Ph.D. Dissertation, University of the Witwatersrand.

Suwa, G., 1988. Evolution of the "robust" australopithecines in the Omo succession: evidence from mandibular premolar morphology. In: Grine, F.E. (Ed.), Evolutionary History of the 'Robust' Australopithecines. Aldine de Gruyter, New York, pp. 199–222.

Suwa, G., 1996. Serial allocations of isolated mandibular molars of unknown taxonomic affinities from the Shungura and Usno formations, Ethiopia, a combined method approach. Human Evolution 11, 269–282.

Suwa, G., White, T.D., Howell, F.C., 1996. Mandibular postcanine dentition from the Shungura Formation, Ethiopia: crown morphology, taxonomic allocations, and Plio-Pleistocene hominid evolution. American Journal of Physical Anthropology 101, 247–282.

Turner, C.G., Nichol, C.R., Scott, G.R., 1991. Scoring procedures for key morphological traits of the permanent dentition: the Arizona State University dental anthro-pology system. In: Kelley, M.A., Larsen, C.S. (Eds.), Advances in Dental Anthro-pology. Wiley- Liss, New York, pp. 13–32.

Vaillant, M., Glaun`es, J., 2005. Surface matching via currents. Information Processing in Medical Imaging 3565, 381–392.

Vaillant, M., Qiu, A., Glaun`es, J., Miller, M.I., 2007. Diffeomorphic metric surface mapping in superior temporal gyrus. Neuroimage 34, 1149–1159.

Villmoare, B., Kimbel, W.H., Seyoum, C., Campisano, C.J., DiMaggio, E.N., Rowan, J., Braun, D.R., Arrowsmith, J.R., Reed, K.E., 2015. Early *Homo* at 2.8 Ma from Ledi-Geraru, Afar, Ethiopia. Science 347, 1352–1355.

von Cramon-Taubadel, N., Frazier, B.C., Lahr, M.M., 2007. The problem of assessing landmark error in geometric morphometrics: theory, methods, and modifications. American Journal of Physical Anthropology 134, 24–35.

Walker, J.A., 2000. Ability of geometric morphometric methods to estimate a known matic Biology 49, 686–696.

Wood, B.A., Abbott, S.A., 1983. Analysis of the dental morphology of Plio-Pleistocene hominids. I. Mandibular molars: crown area measurements and morphological traits. Journal of Anatomy 136, 197–219.

Wood, B.A., Engleman, C.A., 1988. Analysis of the dental morphology of Plio-Pleistocene hominids. V. Maxillary postcanine tooth morphology. Journal of Anatomy 161, 1–35.

Wood, B.A., Uytterschaut, H.T., 1987. Analysis of the dental morphology of Plio-Pleistocene hominids. III. Mandibular premolar crowns. Journal of Anatomy 154, 121–156.

Wood, B., Harrison, T., 2011. The evolutionary context of the first hominins. Nature 470, 347–352.

Wu, C., Murtha, P.E., Jaramaz, B., 2009. Femur statistical atlas construction based on two-level 3D non-rigid registration. Computer Aided Surgery 14, 83–99.

Zanolli, C., Bondioli, L., Mancini, L., Mazurier, A., Widianto, H., Macchiarelli, R., 2012. Two human fossil deciduous molars from the Sangiran Dome (Java, Indonesia): outer and inner morphology. American Journal of Physical Anthropology 147, 472–481.

Zelditch, M., Swiderski, D., Sheets, H., Fink, W., 2004. Geometric Morphometrics for Biologists. A Primer. Elsevier Academic Press, London.